electronics

MDPI

Article

Optimal Energy Storage Allocation for Combined Wind-PV-EVs-ES System Based on Improved Triangulation Topology Aggregation Optimizer

Chuanxi Fan [1,*], Haizheng Wang [2], Jinhua Zhang [1,*], Peng Cheng [3] and Yuhua Bian [1]

[1] School of Electrical Engineering, North China University of Water Resources and Electric Power, Zhengzhou 450045, China; 17513363971@163.com
[2] China Renewable Energy Engineering Institute, Beijing 100120, China; whz@creei.cn
[3] School of Mathematics and Statistics, North China University of Water Resources and Electric Power, Zhengzhou 450045, China; chengpeng@ncwu.edu.cn
* Correspondence: z202210050659@stu.ncwu.edu.cn (C.F.); zhangjh@ncwu.edu.cn (J.Z.)

Abstract: To determine the ES allocation based on a specific number of EVs connected to a combined WPESS, this paper develops an ESS allocation model that considers the impact of EV charging behavior on LSD, ES allocation cost, new energy utilization rate, and self-power rate. First, several scenarios are generated using Monte Carlo sampling (MCS), and a typical day is selected through Backward Reduction (BR). Next, the Monte Carlo method is employed to generate conventional EV charging curves and optimize EV charging behavior by considering LSD and user charging costs. Subsequently, an ES capacity allocation model is developed, considering system costs, new energy utilization rate, and self-power rate. Finally, an improved triangulation topology aggregation optimizer (TTAO) is proposed, incorporating the logistic map, Golden Sine Algorithm (Gold-SA) strategy, and lens inverse imaging learning strategy. These enhancements improve the algorithm's ability to identify global optimal solutions and facilitate its escape from local optima, significantly enhancing the optimization effectiveness of TTAO. The analysis of the calculation example indicates that after optimizing the charging behavior of EVs, the average daily cost is reduced by 204.94, the self-power rate increases by 2.25%, and the utilization rate of new energy sources rises by 2.50%, all while maintaining the same ES capacity.

Keywords: energy storage system; electric vehicle; new energy; triangulation topology aggregation optimizer; multi-objective optimization

Citation: Fan, C.; Wang, H.; Zhang, J.; Cheng, P.; Bian, Y. Optimal Energy Storage Allocation for Combined Wind-PV-EVs-ES System Based on Improved Triangulation Topology Aggregation Optimizer. *Electronics* **2024**, *13*, 4041. https://doi.org/10.3390/electronics13204041

Academic Editor: Gianpaolo Vitale

Received: 13 September 2024
Revised: 9 October 2024
Accepted: 12 October 2024
Published: 14 October 2024

1. Introduction

As greenhouse gas emissions continue to rise annually, China has established a goal for low-carbon development, aiming to reduce carbon emissions [1]. The installed capacity of NE has rapidly increased in recent years. However, the uncertainty of NE output poses a challenge to the power system [2,3]. The volatility and uncontrollability of wind and photovoltaic energy pose significant challenges to the consumption of new energy and contribute to the large-scale abandonment of wind and solar power [4]. Simultaneously, the uncertainty associated with wind and photovoltaic energy, combined with the charging loads of electric vehicles, presents considerable challenges to grid planning. Furthermore, large-scale wind/PV/load exacerbates the complexities of power system planning [5]. The WPEES effectiveness in optimizing energy efficiency and economic benefits depends on a rational configuration of the system and the development of operational programs. An irrational configuration can lead to increased consumption of new energy and resource waste, resulting in more pronounced issues [6,7]. Consequently, addressing the uncertainties of wind (PV) output and load is crucial, as is reducing the generated large-scale scenario set to achieve rational operational planning of the Wind-PV-Electric Vehicle-Energy Storage

System (WPESS). Implementing a well-structured energy storage configuration scheme that accounts for the charging power of electric vehicles can maximize its advantages regarding economy, resources, and the environment [8].

The authors in [9] introduced a cluster analysis method for large-scale scene simplification that is applicable to existing methods and subsequently proposed an improved clustering algorithm. The authors in [10] employed Monte Carlo simulation methods and Copula theory to generate scenarios that account for the interdependence of wind and photovoltaic (PV) power generation, applying a rapid scenario reduction methodology to balance accuracy and computational speed. The authors in [11] suggested that dynamically adjusting EV charging times can maximize the use of wind power, achieve economic operational efficiency, and reduce pollution emissions. The study presented in [12] introduces an MCS-based forecasting method for EV and 'green power' alongside a PV and EV system joint optimization management model. The authors in [13] presented an EV charging scheme designed to accommodate the varying demands of both the grid and users by adjusting the EV charging state and power. In [14], a novel energy management optimization model is proposed based on online reinforcement learning, capable of efficiently learning scheduling strategies for microgrids using the state–action–reward–state–action (SARSA) algorithm. The authors in [15] provided a comprehensive review of ES technologies used in an NE system. In [16], a capacity optimization allocation model for a PV-WT-ES system is examined, aiming to minimize both the cost and the LPSP. The authors in [17] used PSO to determine the size and location of the BESS and used DOPF methods to determine the locations and sizes of renewable energy sources in a spatio-temporal framework aimed at reducing carbon emissions and minimizing costs. In [18], an upper-layer model which aims to minimize energy storage allocation costs is proposed, and the lower-layer model focuses on minimizing system operating costs, incorporating robust optimization theory to address uncertainty. A MOSaDE-based optimization method for a hybrid PV-WT-DD microgrid is proposed in [19]. This method simultaneously considers multiple objectives, including LPSP, COE, and RF, providing a series of Pareto-optimal solutions for system designers.

TTAO [20] was proposed by S. Zhao in 2024 for solving continuous optimization problems and engineering applications. The algorithm utilizes a triangular topology in mathematics to balance exploration and exploitation through two strategies: generic aggregation and local aggregation. TTAO performs well in multidimensional functions and real engineering problems, and its optimization performance is significantly better than many current competing algorithms, making it suitable for solving the allocation of ES capacity.

In this paper, based on the context of EVs connected to the WPESS, we constructed an optimal allocation model of ES capacity, considering the influence of LSD, cost, NE utilization rate, and self-power rate. First, this paper generates several scenarios using Monte Carlo sampling (MCS) and selects a typical day through Backward Reduction (BR). Secondly, the disordered charging curve of electric vehicles (EVs) is generated using the Monte Carlo method, and an ordered charging optimization model for EVs is established, considering the load standard deviation and user charging costs. Then, an energy storage capacity allocation model is established, considering system cost, new energy utilization, and self-power supply rate. Finally, an improved triangulation topology aggregation optimizer (TTAO) based on the logistic map, Golden Sine Algorithm (Gold-SA) strategy, and lens inverse imaging learning strategy is proposed for these models.

The key contributions of this work include the following:

- Generated power-load scenarios using Monte Carlo sampling and selected typical days for subsequent calculations through Backward Reduction;
- Utilized MCS to obtain the EV disorderly charging load and established an orderly charging optimization model for EVs, considering the load standard deviation and the cost of charging to derive the EV orderly charging power;

- An energy storage capacity allocation model is established, considering system cost, new energy utilization rate, and self-powered rate, with energy storage allocation results obtained for both disorderly and orderly EV charging;
- Improved TTAO through the logistic map, Golden Sine Algorithm (Gold-SA) strategy, and lens inverse imaging learning strategy to enhance its local and global optimization capabilities, introducing a Pareto solution set, applying it to multi-objective optimization, and selecting a compromise solution based on TOPSIS method.

The key points of the subsequent sections of this paper are outlined as follows below.

Section 2 introduces the optimized ES allocation model for the WPEES, including a scenario analysis method based on MCS and BR, conventional charging model and sequential charging optimization model for EVs aimed at minimizing LSD and user charging cost, and a multi-objective ES allocation model based on MOITTAO.

Section 3 describes the basic principles of TTAO and the improved strategies, including the logistic map, Golden Sine Algorithm (Gold-SA), and lens inverse imaging learning, introduces the Pareto solution set, and ultimately selects the compromise solution from this set using a fuzzy multi-attribute decision-making method.

Section 4 verifies the feasibility of the model by calculating and analyzing an arithmetic example.

Section 5 provides a comprehensive summary of the text and discusses the results obtained.

2. Optimized Energy Storage Allocation Model

This paper constructs an ES allocation model for the WPEES based on the typical day generated through the MCS and BR method while considering the influence of EV charging behavior. The NE system is illustrated in Figure 1.

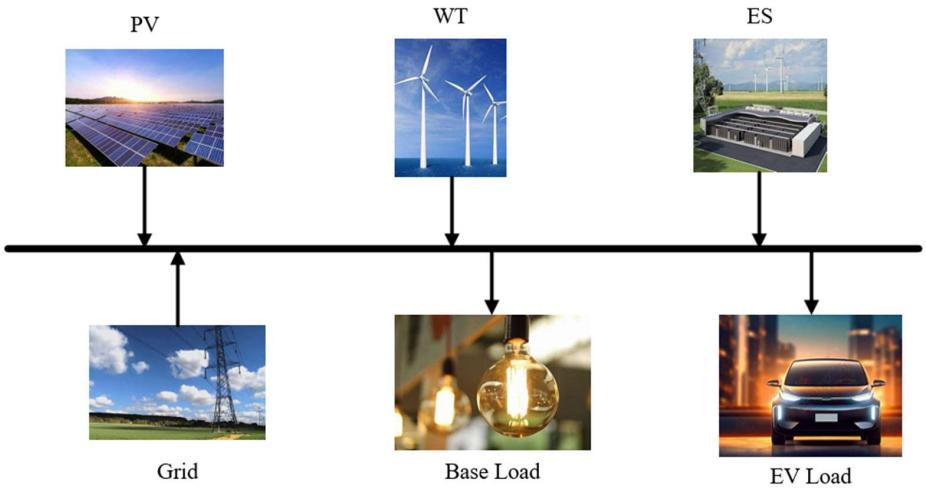

Figure 1. New energy system structure diagram.

2.1. Scenario Analysis Based on MCS and BR

In numerous articles, the fuzzy planning method, opportunity constraint planning method, and scenario analysis method are commonly employed to study the uncertainty of NE output. In this paper, the scenario analysis method is employed to address the uncertainty problem of NE output, which is primarily divided into two components: scenario generation and scenario reduction. The scenario generation method utilizes Monte Carlo simulation (MCS), while the scenario reduction method employs Backward Reduction (BR). MCS is the most widely used method for generating scenarios, known for its simplicity and speed [21,22]. The BR method eliminates scenarios that do not meet specific constraints based on computational distance and iteratively reduces a single scenario until it satisfies the criteria for scenario reduction [23,24].

Uncertainty in wind turbine output primarily arises from the randomness and volatility of wind speed. Wind speed follows the Weibull distribution [25,26]:

$$f(v,c,k) = \frac{k}{c}\left(\frac{v}{c}\right)^{k-1} \exp\left[-\left(\frac{v}{c}\right)^{k}\right] \tag{1}$$

In the formula, v is the actual wind speed; c and k are parameters.

The CDF for the Weibull distribution is as follows [27–29]:

$$F(v;c,k) = 1 - \exp\left[-\left(\frac{v}{c}\right)^{k}\right] \tag{2}$$

PV output power is primarily influenced by solar radiation. Solar radiation follows a Beta distribution over a specific period of time [30,31]:

$$f(s;\alpha,\beta) = \frac{\Gamma(\alpha+\beta)}{\Gamma(\alpha)\Gamma(\beta)} s^{\alpha-1}(1-s)^{\beta-1} \tag{3}$$

In the formula, s is the solar radiation intensity; β is the shape parameters.

The load is treated according to a normal distribution.

The wind power scenario can be obtained from the probability distribution of wind speed:

$$P_{\mathrm{w}} = \begin{cases} 0, v < v_{in}, v > v_{\mathrm{out}} \\ P_{\mathrm{w},r}, v_{\mathrm{n}} \leqslant v \leqslant v_{\mathrm{out}} \\ (v - v_{\mathrm{in}})P_{\mathrm{w},r}/(v_{\mathrm{n}} - v_{\mathrm{in}}), v_{\mathrm{in}} \leqslant v \leqslant v_{\mathrm{n}} \end{cases} \tag{4}$$

In the formula, v_n, v_{in}, and v_{out} are wind speeds; P_w denotes the rated power and output power, respectively.

Similarly, the PV scenario can be obtained:

$$P_{\mathrm{PV}} = sA_{\mathrm{PV}}\eta_{\mathrm{PV}} \tag{5}$$

In the formula, P_{PV} is the photovoltaic output power; s is the photovoltaic radiation area; A_{PV} is the maximum light intensity; and η_{PV} is the photovoltaic conversion efficiency.

The MCS method generates a substantial amount of data, characterized by a high degree of similarity among the scenarios. To merge similar scenarios more efficiently, this paper employs BR to reduce scenarios to five and constructs typical day scenarios for wind, PV, and load, taking into account uncertainty based on the weights of these five scenarios. Figure 2 presents the flowchart of the scenario analysis model.

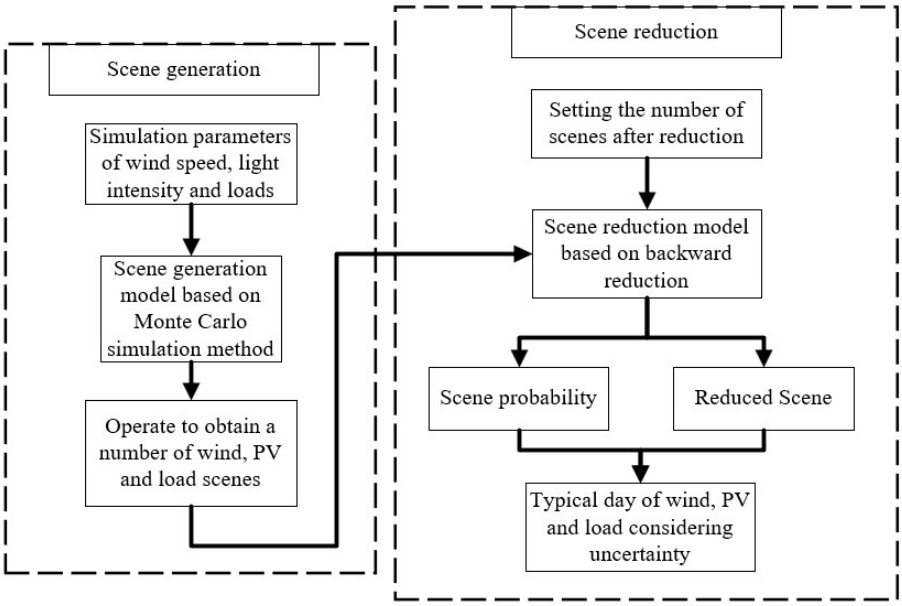

Figure 2. Flowchart of the scenario analysis model.

2.2. Model for EV Charging

This paper develops a charging load model for electric vehicles (EVs) using statistical methods. By randomly extracting specific EV charging data, we design a statistical model based on user travel behavior to generate independent load curves for each electric vehicle (EV). These independent charging load curves are then superimposed to derive the overall EV charging load curve. This study employs the Monte Carlo method, accounting for daily driving mileage, initial state of charge, and charging time of EVs, to establish the EV charging load model.

2.2.1. EV Disorderly Charging Model

Users primarily utilize electric vehicles (EVs) for daily commuting, and their daily mileage exhibits both regularity and variability. Referring to the U.S. 2017 National Statistical Analysis of Vehicle Travel Data (NHT2017) [32], it is assumed that the daily mileage traveled by EV users approximates a lognormal distribution with the following probability density function [12]:

$$f_{\mathrm{D}}(x) = \frac{1}{x\sigma_{\mathrm{D}}\sqrt{2\pi}} \exp[-\frac{(\ln x - \mu_{\mathrm{D}})^2}{2\sigma_{\mathrm{D}}^2}] \tag{6}$$

In the formula, x is the daily mileage of an EV; μ_{D} is the expected value, μ_{D} = 3.20; σ_{D} is the standard deviation of the logarithm of daily mileage, σ_{D} = 0.88.

When the electric vehicle (EV) owner begins charging immediately upon reaching their destination, the final return time of the vehicle corresponds to the initial charging time, which follows a normal distribution characterized by the following probability density function [12,33]:

$$f(T_{\mathrm{r}}) = \begin{cases} \frac{1}{\sqrt{2\pi}\sigma_{\mathrm{r}}} \exp[-\frac{(T_{\mathrm{r}}-\mu_{\mathrm{r}})^2}{2\sigma_{\mathrm{r}}^2}], \mu_{\mathrm{r}} - 12 < T_{\mathrm{r}} \leq 24 \\ \\ \frac{1}{\sqrt{2\pi}\sigma_{\mathrm{r}}} \exp[-\frac{(T_{\mathrm{r}}+24-\mu_{\mathrm{r}})^2}{2\sigma_{\mathrm{r}}^2}], 0 < T_{\mathrm{r}} \leq \mu_{\mathrm{r}} - 12 \end{cases} \tag{7}$$

In the formula, T_{r} is the initial charging time of EV; μ_{r} is the expected value, μ_{r} = 17.60; σ_{r} is the standard deviation, σ_{r} = 3.40.

The charging of electric vehicles (EVs) ceases upon reaching the upper limit of battery capacity. The amount of power consumed is primarily related to the mileage traveled, and the charging duration of an EV is calculated using the following formula:

$$T_{\mathrm{c}} = \frac{x_i \cdot p_{ev}}{P_{\mathrm{c}} \cdot \eta_{\mathrm{c}}} \tag{8}$$

In the formula, T_{c} is the time required for charging; x_i is the mileage traveled by the i-th vehicle; p_{ev} is the power consumption per kilometer of the electric vehicle; η_{c} is the charging power and energy conversion efficiency, respectively.

2.2.2. EV Orderly Charging Optimization Model

Implementing time-sharing tariffs enhances the economic efficiency of electricity pricing by imposing higher tariffs during peak consumption hours and lower tariffs during off-peak hours. This approach effectively reduces the load standard deviation, lowers generation costs, and enhances overall economic efficiency. This paper adopts time-sharing tariffs and develops various orderly charging models for electric vehicles (EVs) based on V2G technology. On the grid side, the primary objective is to reduce the load standard deviation and mitigate load fluctuations. Conversely, on the user side, the main goal is to minimize charging costs for users participating in V2G services, significantly increasing their willingness to engage. The decision variable is the magnitude of power exchanged between EVs and the grid during each time slot. A triangular topology optimizer is

employed to optimize EV charging behavior, and the strategy's effectiveness is evaluated by comparing it to a disordered charging scenario [33].

(1) Objective Function

1. The V2G control strategy for EV participation on the grid side focuses on assisted peaking. It divides the day into 24 time segments, with the charging behavior of EVs in each segment serving as the decision variable. Minimize the LSD as follows:

$$\min D = \mathrm{std}(P_i) \tag{9}$$

$$P_i = P_{i,c} + P_{i,v} \tag{10}$$

In the formula, P_i is the load; $P_{i,c}$ is the EV charging load; $P_{i,v}$ is the base load; and D is the objective function of the optimization.

2. EVs can exchange power with the grid at each time slot, converting this exchanged energy into monetary terms based on electricity prices. Considering time-of-use tariffs, the rates for each period vary, and the V2G control strategy for EV participation on the user side prioritizes economic efficiency. The function is formulated to minimize charging costs during peak and off-peak hours for EV participation in the grid:

$$\min S_t = \sum_{i=1}^{24} (P_{i,c} \cdot Q_i) \tag{11}$$

In the formula, Q_i is the tariff for the time period i.

3. Linear weighting

Based on the linear weighted sum method, the objective functions are normalized with the following equations:

$$\begin{cases} \min S = \lambda_{k,1}\left(\frac{D - D^{\min}}{D^{\max} - D^{\min}}\right) + \lambda_{k,2}\left(\frac{S_t - S_t^{\min}}{S_t^{\max} - S_t^{\min}}\right) \\ \lambda_{k,1} + \lambda_{k,2} = 1 \end{cases} \tag{12}$$

In the formula, S is the multi-objective optimization function of EVs; $D^{\max}$, $S_t^{\max}$ are the maximum values of D, S_t, respectively; $D^{\min}$, $S_t^{\min}$ are the minimize values of D, S_t, respectively; $\lambda_{k,1}$, $\lambda_{k,2}$ are the weights, respectively.

(2) Restrictive Condition

1. Minimum SOC when the user leaves the constraint

The user can establish a minimum battery capacity, ensuring that the vehicle has at least 30% remaining to meet trip power demands. The constraint is as follows:

$$SOC_{it} \geq 0.3 \tag{13}$$

2. Charging time constraint

$$T_s \leqslant T \leqslant T_{\mathrm{e}} \tag{14}$$

In the formula, T_s is the beginning of the regulation period; T_{e} is the end of the regulation period.

3. Total power constraint

$$S = \sum_{i}^{N_g} P_i * T_c^i \tag{15}$$

In the formula, N_g is the number of EVs; T_c^i is the charging time required for *ith* EV.

4. Charging behavioral constraint

The same electric vehicle can only be in a charging or discharging state at the same time.

Figure 3 illustrates the EV's orderly and disorderly charging model.

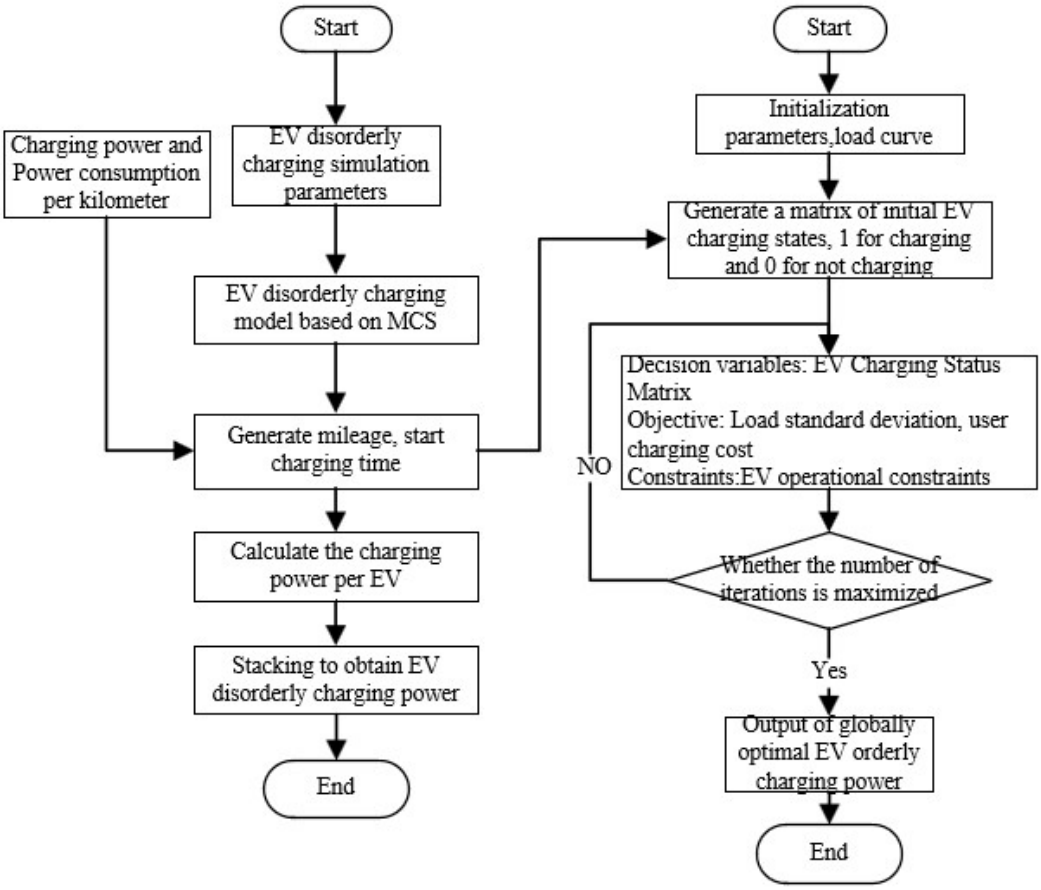

Figure 3. Flowchart of the EV charging model.

2.3. ES Capacity Allocation Model

Various ES devices are available, with chemical energy storage providing advantages such as simplicity, speed, and high conversion efficiency. Batteries, as a method of chemical energy storage, have been widely applied. The ESS for wind and PV is designed to utilize BESS. Due to their flexible charging and discharging capabilities, batteries can adaptively coordinate the power of other generation units within the system, effectively suppressing intermittent renewable energy while achieving peak shaving and valley filling. The mathematical model for this is presented as follows:

$$E_{es}(t) = E_{\mathrm{es}}(t-1) + \left(P_{\mathrm{es,chr}}(t)\eta_{\mathrm{es,chr}} - \frac{P_{\mathrm{es,disch}}(t)}{\eta_{\mathrm{es,disch}}} \right) \Delta t \tag{16}$$

In the formula, E_{es} is the SOC of the battery/kWh; $P_{\mathrm{es,chr}}$ is the charging power/kW; $P_{\mathrm{es,disch}}$ is the discharging power/kW; $\eta_{\mathrm{es,chr}}$ and $\eta_{\mathrm{es,disch}}$ are the efficiency.

The model aims to develop a configuration scheme for the rated capacity of ES, defining the ES rated capacity and the SOC of the ES at each moment as the decision variable in the optimization problem. The ES capacity allocation model is developed based on three evaluation indices: the system self-powered rate, total investment cost, and new energy utilization rate [34].

2.3.1. Objective Function

(1) Minimize the average daily cost

The cost of the ESS primarily consists of the initial construction cost and periodic O&M costs. Additionally, power must be purchased from the grid when the combined output from wind power, photovoltaics, and battery discharges is insufficient to meet compliance demand. As optimal scheduling is conducted for a typical day, the initial investment and periodic O&M costs are averaged over that day.

The average daily cost includes the ES installation cost, the O&M cost, and purchased electricity cost [35]:

$$\min C_t = C_0 + C_{op} + C_{np} \tag{17}$$

In the formula, C_0 is the ES cost; C_{op} is the system O&M cost; C_{np} is purchase electricity cost.

The average daily cost of the ESS is as follows:

$$C_0 = E_{BESS} * k_{BESS} * \frac{l(l+1)^n}{(l+1)^n - 1} / 365 \tag{18}$$

In the formula, C_0 is the average daily cost; E_{BESS} is installed capacity of ES; k_{BESS} is the unit capacity cost; n is the useful life of ES equipment; l is the discount rate.

The cost of regular O&M is directly proportional to the construction cost of the ES system:

$$C_{op} = \lambda C_0 \tag{19}$$

In the formula, λ represents the O&M rate of the ESS cost.

The system is connected to a large power grid, and if an imbalance occurs between power supply and demand, power must be purchased from the grid, resulting in additional'costs:

$$C_{np} = \sum_{1}^{T} (Q_{grid}^t * P_{grid}^t * \Delta t) \tag{20}$$

In the formula, Q_{grid}^t represents the price; P_{grid}^t is the power purchased from the grid.

(2) Maximize system self-power rate

The self-supply rate refers to the proportion of load power met by wind power, photovoltaics, and storage battery discharges relative to the total load demand within the system. This metric reflects the reliability of the new energy power supply and is influenced by new energy output, load demand, and ES [36,37]. The maximum target for the self-supply rate of the system is expressed as follows:

$$\max R_{self} = 1 - \sum_{t=1}^{T} P_{grid}^t / \sum_{t=1}^{T} (L_s^t + P_{es.chr}^t) \tag{21}$$

In the formula, P_{grid}^t is the purchased power; L_s^t is the load; $P_{es.chr}^t$ is the charging power of ESS.

(3) Maximize utilization of new energy

When system power supply exceeds demand, it can lead to power abandonment. The new energy utilization rate refers to the proportion of power (including ES charging) from new energy generation that occurs after power abandonment. A higher new energy utilization rate indicates less power abandonment [38]. The maximum target for the NE utilization rate is expressed as follows:

$$\max G = \frac{\sum_{t=1}^{T}\left(p_{pv}^{t} + p_{wt}^{t}\right)}{P_{out}} \tag{22}$$

In the formula, p_{pv}^{t} is the PV consumed in the time period t, kWh; p_{wt}^{t} is the wind power consumed in the time period t, kWh; $P_{out} = P_{wt} + P_{pv}$ is the total new energy generation, kWh.

2.3.2. Restrictive Condition

(1) SOC constraint

The SOC is defined as the ratio of the power currently stored in the ESS to its storage capacity:

$$SOC(t) = \frac{E_{es}(t)}{E_{BESS}} \tag{23}$$

In the formula, $SOC(t)$ is the ES state; E_{BESS} is the rated capacity.

To ensure the battery's lifetime, upper and lower limits should be established for the SOC:

$$0.2 \leq SOC \leq 0.9 \tag{24}$$

(2) ESS capacity constraint

The upper and lower capacity limits of the energy storage system should be predefined in calculating the optimal configuration of the system.

$$E_{BESS,\,min} \leq E_{BESS} \leq E_{BESS,\,max} \tag{25}$$

In the formula, $E_{BESS,\,max}$ and $E_{BESS,\,min}$ are the minimum and maximum capacity of the storage system, respectively.

(3) Charge/discharge power constraint

$$\begin{aligned} 0 \leq P_{es,ch} \leq P_{es,ch}^{\max} \\ 0 \leq P_{es,disch} \leq P_{es,disch}^{\max} \end{aligned} \tag{26}$$

In the formula, $P_{es,ch}^{\max}$ the maximum value of the charging power of the ESS; $P_{es,disch}^{\max}$ is the maximum value of the discharging power of the ESS.

(4) Power balance constraint

The power supply and consumption of the entire system must ensure energy conservation; therefore, power balance constraints need to be established.

$$P_{wt}^{t} + P_{pv}^{t} + P_{es,disch}^{t} + P_{grid}^{t} = P_{L}^{t} + P_{es,ch}^{t} + P_{loss}^{t} \tag{27}$$

In the formula, P_{wt}^{t} is the wind power output, kW; P_{pv}^{t} is the photovoltaic output, kW; $P_{es,disch}^{t}$ is the discharging power of the battery, kW; P_{grid}^{t} is the power purchased from the grid, kW; P_{L}^{t} is the load power, kW; $P_{es,ch}^{t}$ is the ESS charging power, kW; P_{loss}^{t} is the power discarded by NE.

The flowchart for optimal allocation of ES is shown in Figure 4.

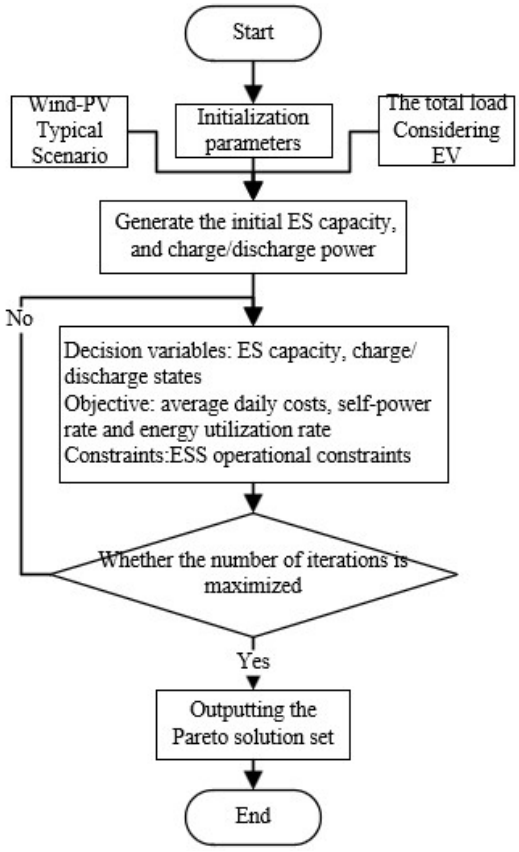

Figure 4. Flowchart of ES allocation and operation optimization.

The flowchart of the optimized ES configuration is shown in Figure 5.

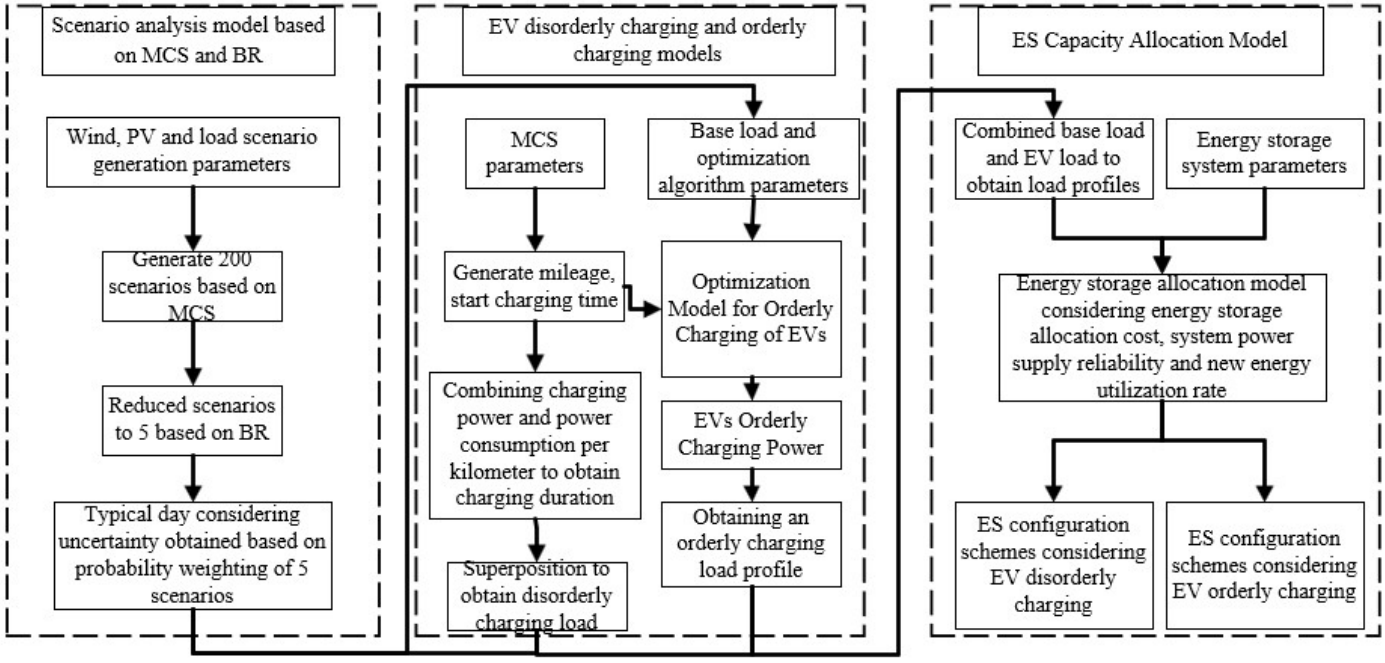

Figure 5. Flowchart of Wind-PV-EVs-ES system.

3. Triangulation Topology Aggregation Optimizer

The TTAO [20] was proposed by S. Zhao in 2024. The TTAO is based on the concept of similar triangles. The TTAO consists of a population initialization phase, a triangle topology unit formation phase, a global aggregation phase, and a local aggregation phase.

3.1. Mathematical Model of TTAO

(1) Population initialization

First, the TTAO initializes the population based on the specified population size N and variable dimension D. The N individuals are grouped into $N/3$ triangular topological units, with the remaining individuals being randomly distributed. During initialization, $N/3$ search agents are randomly generated within the allowed range, and each agent is generated using the following formula:

$$X_{i,1} = r_0 \times (UB - LB) + LB \tag{28}$$

In the formula, $X_{i,1}$ denotes the first search individual in the ith triangular topological cell and is a positive integer between 1 and N/3; r_0 denotes a random number between [0, 1]; $\overrightarrow{LB}$ and $\overrightarrow{UB}$ are the lower and upper bounds of the variables.

(2) Triangular topological unit formation stage

Starting from the first vertex of the spherical coordinate system, a new direction vector is established and transformed into the Cartesian coordinate system to create the second vertex. This vector is then rotated counterclockwise by $\pi/3$ and transformed to obtain the third vertex. The mathematical expression for the vertex is as follows:

$$X_{i,2} = X_{i,1} + l * f(\theta) \tag{29}$$

$$X_{i,3} = X_{i,1} + l * f\left(\theta + \frac{\pi}{3}\right) \tag{30}$$

In the formula, l denotes the size of the triangular topological unit, mathematically denoted as $l = 9 * e^{-\frac{t}{T}}$; t denotes the current iteration; T denotes the maximum iteration, which l decreases as iterations increases.

$f(\theta)$ and $f\left(\theta + \frac{\pi}{3}\right)$ denote the direction vectors of the other two edges guided by the first point:

$$f(\theta) = [\cos\theta_1, \cos\theta_2, \ldots, \cos\theta_{D-1}, \cos\theta_D] \tag{31}$$

$$f\left(\theta + \frac{\pi}{3}\right) = \left[\cos\left(\theta_1 + \frac{\pi}{3}\right), \ldots, \cos\left(\theta_{D-1} + \frac{\pi}{3}\right), \cos\left(\theta_D + \frac{\pi}{3}\right)\right] \tag{32}$$

In the formula, $\theta = [\theta_1, \cdots, \theta_D]$ and $\theta_j (j = 1, \cdots, D)$ are random numbers between $[0, \pi]$.

Each set of triangular topological cells is internally aggregated to a fourth vertex. This point is formed as a linear weighting of the other three points, defined as follows:

$$X_{i,4} = r_1 * X_{i,1} + r_2 * X_{i,2} + r_3 * X_{i,3} \tag{33}$$

In the formula, r_1, r_2, and r_3 are random numbers between [0, 1], $r_1 + r_2 + r_3 = 1$. Thus, the fourth vertex is located within each triangular topological cell.

(3) Generic (global) aggregation stage

In the current phase, the algorithm produces a new solution by integrating the information from the best individuals of each triangular cell. This is accomplished by linearly weighting the variables of the two leading individuals:

$$X_{i,new1}^{t+1} = r_4 * X_{i,best}^{t} + (1 - r_4) * X_{rand,best}^{t} \tag{34}$$

In the formula, r_4 is a random number between [0, 1]; $X^t_{i,best}$ and $X^t_{rand,best}$ denote the best individual for the cell and the randomly selected cell at the iteration.

The greedy strategy is used to update the optimal individual, and the mathematical expression is as follows:

$$\begin{cases} X^{t+1}_{i,best} = X^{t+1}_{i,new1} & f_{X^{t+1}_{i,new1}} < f_{X^t_{i,best}} \\ X^{t+1}_{i,sbest} = X^{t+1}_{i,new1} & f_{X^{t+1}_{i,new1}} < f_{X^t_{i,sbest}} \end{cases} \tag{35}$$

The formula $X^{t+1}_{i,sbest}$ denotes the suboptimal individual at the tth iteration.

(4) Local aggregation

During the local aggregation phase of the TTAO algorithm, search optimization within a local region is accomplished by creating a temporary non-equilateral triangular structure around the optimal individual and adjusting its position based on the vector difference with the suboptimal individual. This process aims to enhance the search efficiency of each topological unit while avoiding local optimal solutions. By comparing the fitness values before and after the perturbation, a decision is made on whether to update the position to ensure the effectiveness of the search direction. The new vertex is computed as follows:

$$X^{t+1}_{i,new2} = X^{t+1}_{i,best} + \alpha * \left(X^{t+1}_{i,best} - X^{t+1}_{i,sbest} \right) \tag{36}$$

$$\alpha = \ln\left(\frac{e - e^3}{T - 1} t + e^3 - \frac{e - e^3}{T - 1} \right) \tag{37}$$

To prevent the optimal individual from becoming trapped in a local optimum, the algorithm leverages the data from the suboptimal individual. Throughout the convergence process, it is ensured that the bootstrap points of the temporary triangular cells remain optimal. The decision to update the position is made by comparing the fitness values before and after the local search: if the fitness improves, the position is updated; otherwise, it remains unchanged. The corresponding mathematical formula is as follows:

$$X^{t+1}_{i,best} = \begin{cases} X^{t+1}_{i,new2} & f_{X^{t+1}_{i,new2}} < f_{X^{t+1}_{i,best}} \\ X^{t+1}_{i,best} & otherwise \end{cases} \tag{38}$$

3.2. Algorithmic Improvements

A logistic map is introduced during the population initialization phase of the TTAO, and the generated sequence of random numbers is used to replace the values in Equation (27), thereby enhancing the diversity and randomness of the population, reducing the optimization search time, and accelerating the convergence speed of the algorithm [39]. The logistic map is as follows:

$$z_{k+1} = \mu z_k (1 - z_k) \tag{39}$$

In the formula, $z_0 \notin \{0, 0.25, 0.5, 0.75, 1.0\}$, $\mu \in [0, 4]$, $z_k \in (0, 1)$, $\mu \in [0, 4]$.

Gold-SA is a meta-heuristic optimization algorithm proposed in 2017, inspired by the spatial search performed within the unit circle of the sinusoidal function, akin to the solution of the optimization problem, while shrinking the search space by the golden ratio to approximate the optimal solution [40]. The golden section search is employed in the TTAO generic (global) aggregation process, with the optimal solution updated using a greedy strategy to strike a balance between 'search' and 'development.'

$$x_1 = \pi * (1 - t) - \pi * t \tag{40}$$

$$x_2 = \pi * t - \pi * (1 - t) \tag{41}$$

$$X^{t+1}_{i,new1} = X^t_i * |\sin(R_1)| - R_2 * \sin(R_1) * \left| x_1 * X^t_{i,best} - x_2 * X^t_{rand,best} \right| \tag{42}$$

In the formula, x_1 and x_2 are the golden section coefficients; τ is the golden section rate, $t = (\sqrt{5}-1)/2$; $X^t_{i,best}$ and $X^t_{rand,best}$ are the best individuals for cell and the randomly selected cell; R_1 is the random number between $[0, 2\pi]$, and R_2 is the random number between $[0, \pi]$.

During TTAO local aggregation, lens imaging is used to generate the inverse position $X^{t+1}_{i,new2}$. This allows for jumping out of the current position as well as expanding the search range [41,42].

$$X^{t+1}_{i,new2}{}^{*} = \frac{a_j + b_j}{2} + \frac{a_j + b_j}{2k} - \frac{X^{t+1}_{i,new2}}{k} \tag{43}$$

In the formula, $X^{t+1}_{i,new2}{}^{*}$ is the inverse solution of $X^{t+1}_{i,new2}$; a_j and b_j are the maximum and minimum boundaries of the search space, respectively; k is the scaling factor.

Introducing a dynamically changing $k = \left(1 + (t/T)^{1/2}\right)^{10}$, as iterations increase, the value will become larger, and the range of its inverse solution will become smaller. Also considering that the resulting inverse solution is not necessarily better than the original solution, a greedy strategy is introduced so that the replacement is performed only when the inverse solution is better than the original solution.

3.3. ITTAO-Specific Processes

The mathematical modeling of the ITTAO can be summarized in the following steps:

(1) Input the population size, iterations, and variable dimensions;
(2) Initialize the population using logistic mapping in the population initialization phase;
(3) Generate triangular topological units and calculate the fitness values to find the optimal and suboptimal points in each triangular topological unit;
(4) In the generic (global) aggregation phase, the golden sine strategy is fused to create new feasible solutions, and greedy substitution is used to select the better solution;
(5) In the local aggregation, introduce lens imaging reverse learning to generate a reverse position to expand the search range of the position update, and update the position if the new individual is better than the original one; otherwise, do not perform the update;
(6) Loop this process until the optimal solution under the current constraints is obtained or the upper limit of the number of iterations is reached.

3.4. Multi-Attribute Decision-Making Method

TOPSIS is a method used to select a compromise solution among multiple alternatives based on various objective criteria. It ranks the criterion coefficients of each alternative under each objective criterion and identifies the one with the highest value as the optimal compromise solution. In this paper, to rationally select the compromise solution for ESS allocation, we employ the TOPSIS method, with the specific formula expressed as follows [43]:

$$\mu^k_j = \frac{f^k_j - f^{\min}_j}{f^{\max}_j - f^{\min}_j} \tag{44}$$

$$\mu^k = \frac{\sum_{j=1}^{n} \mu^k_j}{\sum_{k=1}^{m}\sum_{j=1}^{n} \mu^k_j} \tag{45}$$

$$opt = \left\{ o \middle| \quad \mu^o = \max\left(\mu^k\right) \right\} \tag{46}$$

Equation (44) is the normalization of the data, on the basis of which the attribute values of each solution under different objective criteria are summed up by Equation (45), and their share in the sum of attribute values of all solutions under each objective criterion is determined.

4. Calculus Analysis

4.1. Basic Parameters

To verify the validity and applicability of the optimization methodology proposed in this paper, the developed model was implemented using MATLAB R2022a. The test environment incorporates an i5-11400H CPU @ 2.70 GHz and 16 GB of RAM.

(1) Basic Parameters for Scenario Generation

The rated power of wind energy is 800 kW, the rated wind speed is 13 m/s, and the cut-in and cut-out wind speeds are 3 m/s and 25 m/s, respectively. The rated capacity of PV systems is 800 kW, the base value of light intensity is 2, and the rated light intensity is 0.7 kW/m².

(2) Basic Parameters for EV Charging Behavior Optimization

In this study, it is assumed that 200 electric vehicles (EVs) will participate in charging, starting with constant power after their last return trip until fully charged. The specifications of the EVs' power batteries are standardized: the battery capacity is 35 kWh, and the charging power is 5 kW, power consumption is 13.2 kWh per 100 km, and both the battery charging efficiency and energy conversion efficiency are 0.95. The time-sharing tariff is shown in Table 1.

Table 1. Time-sharing tariff.

Time	0:00–7:00	7:00–8:00	8:00–11:00	11:00–18:00	18:00–21:00	21:00–0:00
Tariff/CNY	0.25	0.42	0.82	0.42	0.88	0.42

The typical daily load data from the first section serve as the baseline for solving the EV charging load optimization problem, with a population size of 200 and the number of iterations set to 1000.

(3) Basic Parameters of Energy Storage Capacity Configuration

This study employs the typical daily data from wind turbines, photovoltaic systems, and load obtained in the first part. The state of charge (SOC) of the battery energy storage varies within the range of [0.1, 0.9]; the initial energy storage state is denoted by $0.5E_{BESS}$, and the initial and final charging states of the battery during the day remain essentially the same. The lower limit of the storage configuration capacity is set to 100, while the upper limit is set to 10,000, and the upper limit of ESS power is set to $0.3E_{BESS}$. The specific parameters of the main equipment in the battery storage system are presented in Table 2, while the purchased power tariffs from the local grid are provided in Table 1.

Table 2. Basic parameters of the ESS.

Parameter	Value	Parameter	Value
The unit cost of capacity	1300/kWh	Charging efficiency	0.95
Operating rate	0.1	Discharge efficiency	0.95
Discount rate	0.05	Service life	10 years

The number of iterations and populations for all optimization algorithms are set to 1000 and 300, respectively, establishing the size of the non-inferior solution set to 100. The inertia weight of MOPSO is 0.5, and the weights for both individual optimum and global optimum are set to 2. The grid division is set to 5, and the speed range is defined as $[-1, 1]$. The maximum allowable wastage for MOWOA is set to 50.

4.2. Results Analysis of Scenario Generation and Reduction

This paper employs the MCS method for generating wind and PV scenarios, setting the number of scenarios to 200, and reducing the wind, PV, and load scenarios to 5 using

the BR method. The results of the generation and reduction of wind power, PV, and load scenarios are presented in Figures 6–8.

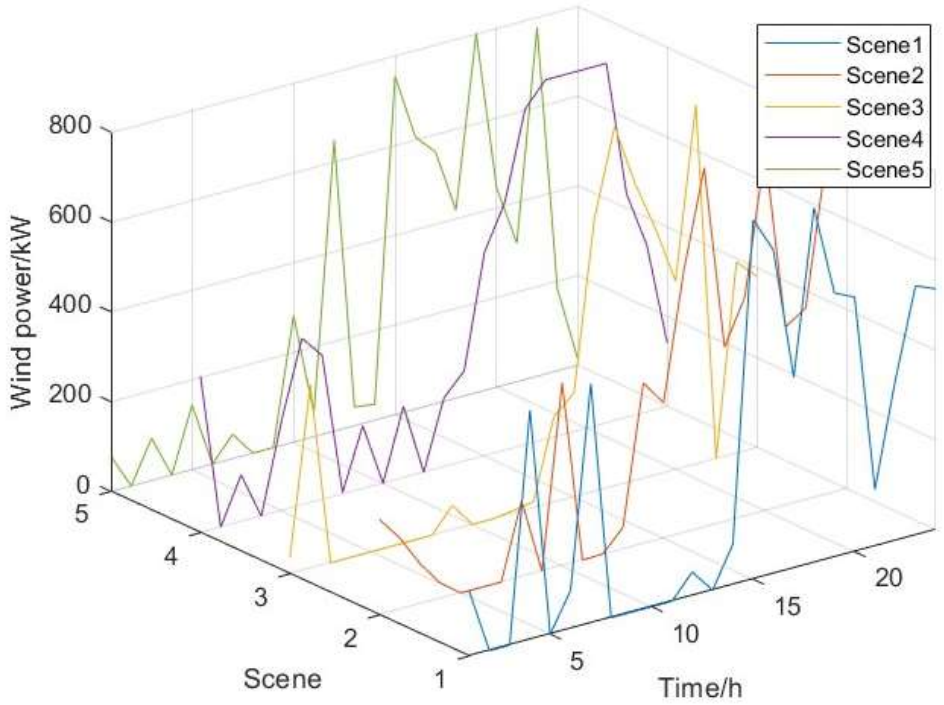

Figure 6. Wind scenarios after reduction.

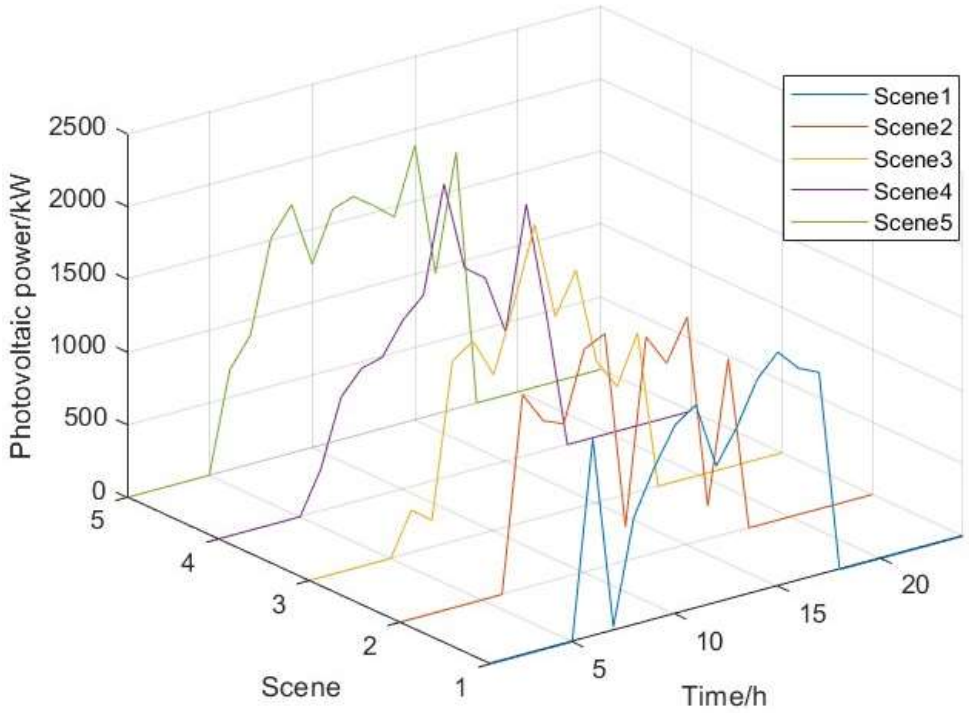

Figure 7. PV scenarios after reduction.

The probabilities of the five scenarios are presented in Table 3, and these scenarios are weighted according to their probabilities to construct typical days. A typical wind-PV-Load scene is illustrated in Figure 9.

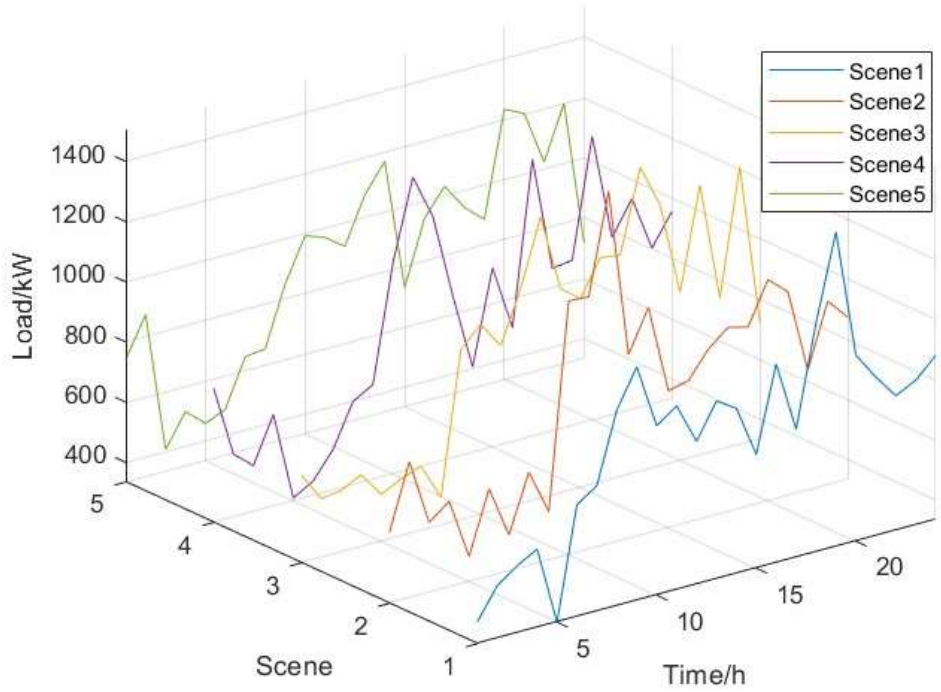

Figure 8. Load scenarios after reduction.

Table 3. Probability of scenarios.

Scene	Scene1	Scene2	Scene3	Scene4	Scene5
Probability	10.5%	9.0%	29.5%	33.0%	18.0%

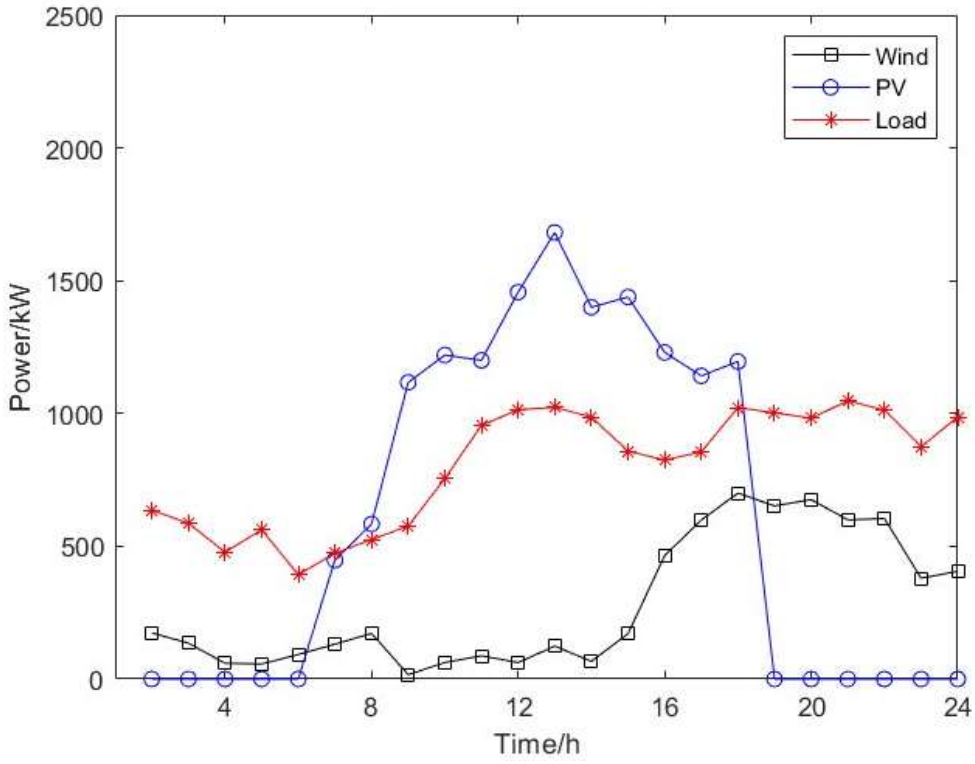

Figure 9. Typical Wind-PV-Load scene.

4.3. Results Analysis of EV Charging

Table 4 presents the optimized load standard deviation and user charging costs, Figure 10 illustrates the power curves for both disorderly and orderly EV charging, and Figure 11 displays the base load curve alongside the EV load curves for disorderly and orderly charging. The analysis indicates that the peak charging power of EVs during disorderly charging occurs around 20:00, coinciding with a relatively high base load, which contributes to an increased mean square deviation of the load curve. The peak charging loads for the optimized charging strategy occur around 6:00 and 16:00, during which both tariffs and base load are relatively low, allowing for a significant reduction in load standard deviation and user charging cost.

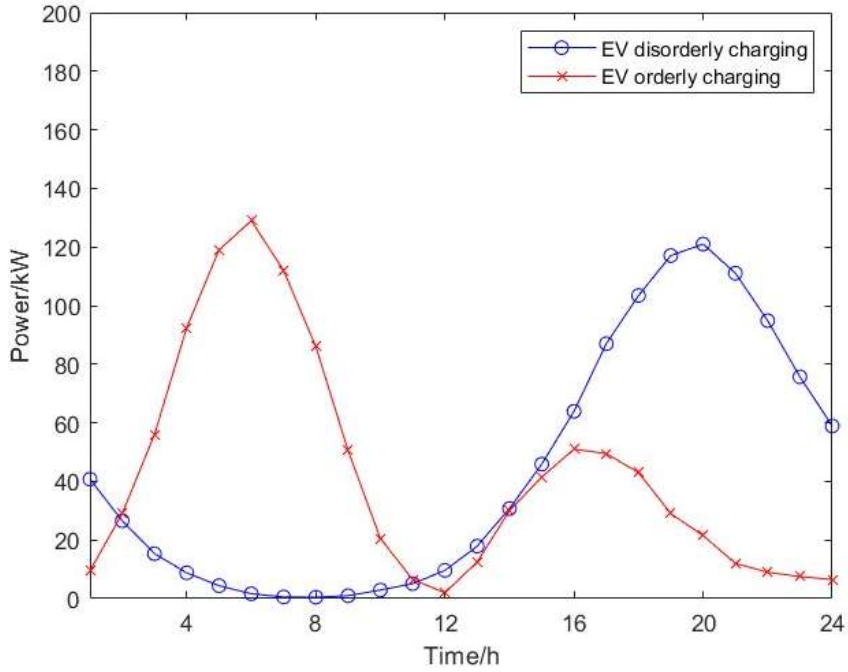

Figure 10. EV disorderly and orderly charging power.

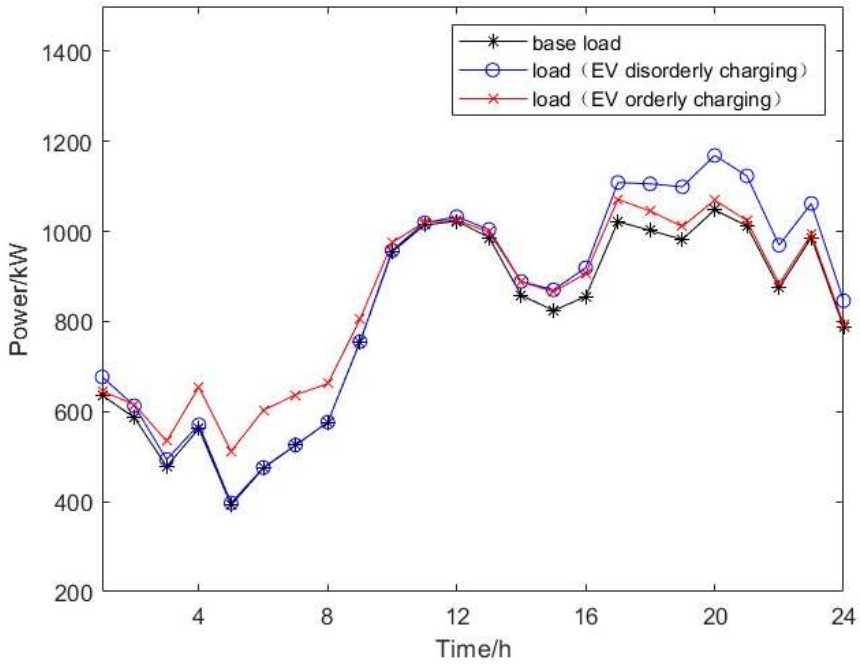

Figure 11. Load curves.

Table 4. Load standard deviation and user charging cost.

Mode	Charging Costs/CNY	Load Standard Deviation/kW
Base load	-	215.14
EV disorderly charging	579.45	243.10
EV orderly charging	259.13	158.96

4.4. Results Analysis of Optimized Allocation of ES

In this study, three distinct scenarios were developed for comparative analysis aimed at assessing the validity of the model:

(1) Scenario 1: EVs using disorderly charging mode with no energy storage configuration;
(2) Scenario 2: EVs using disorderly charging mode, configured with energy storage;
(3) Scenario 3: EVs using orderly charging mode, configured with energy storage.

The iteration curves for multi-objective optimization related to Scenario 3, employing various optimization algorithms for each objective, are illustrated in Figures 12–14, while the Pareto solution is depicted in Figure 15.

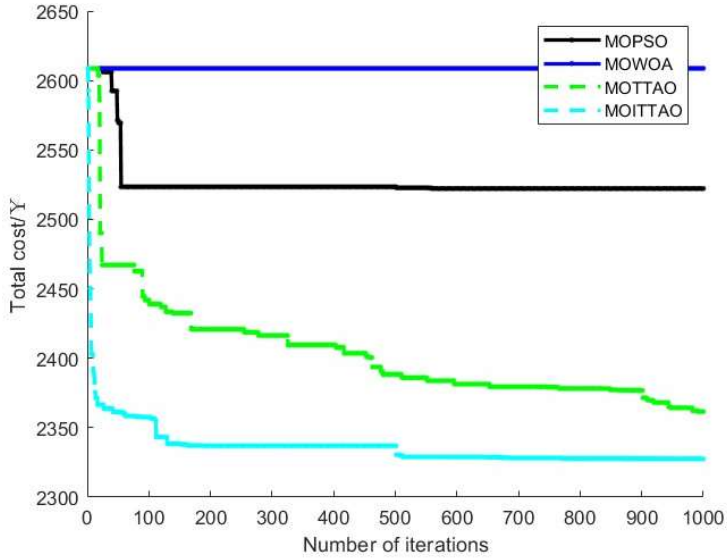

Figure 12. Average daily investment comparison.

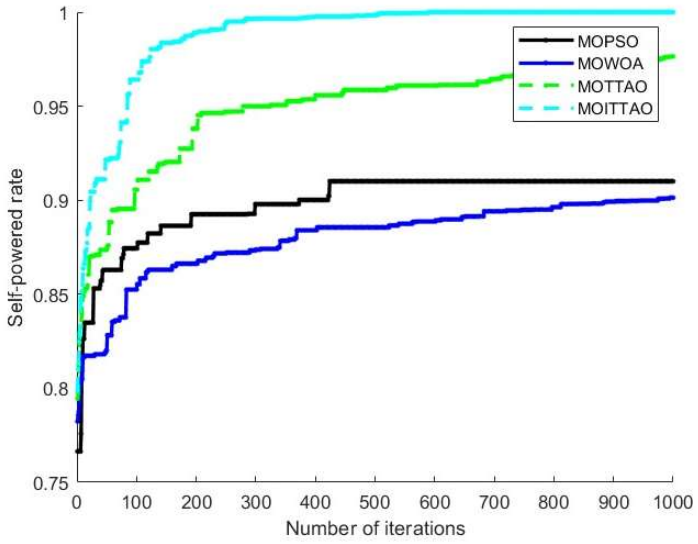

Figure 13. Self-powered rate comparison.

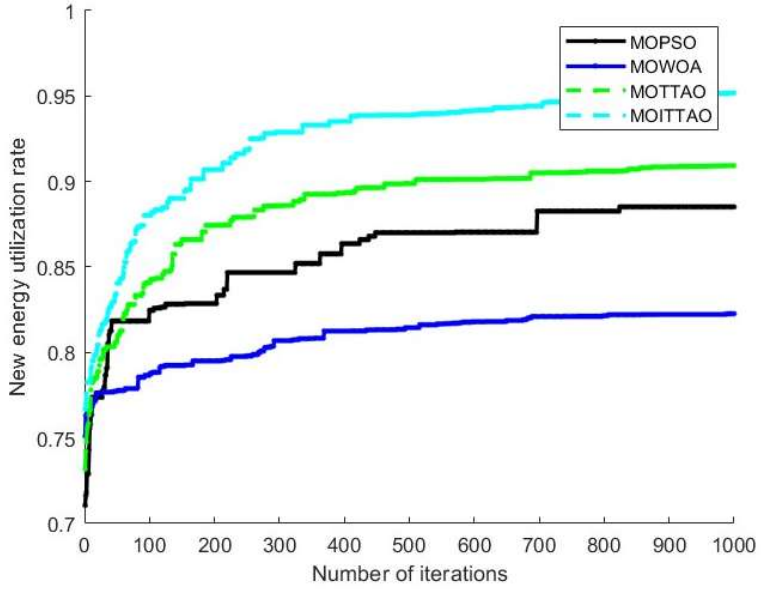

Figure 14. New energy utilization rate comparison.

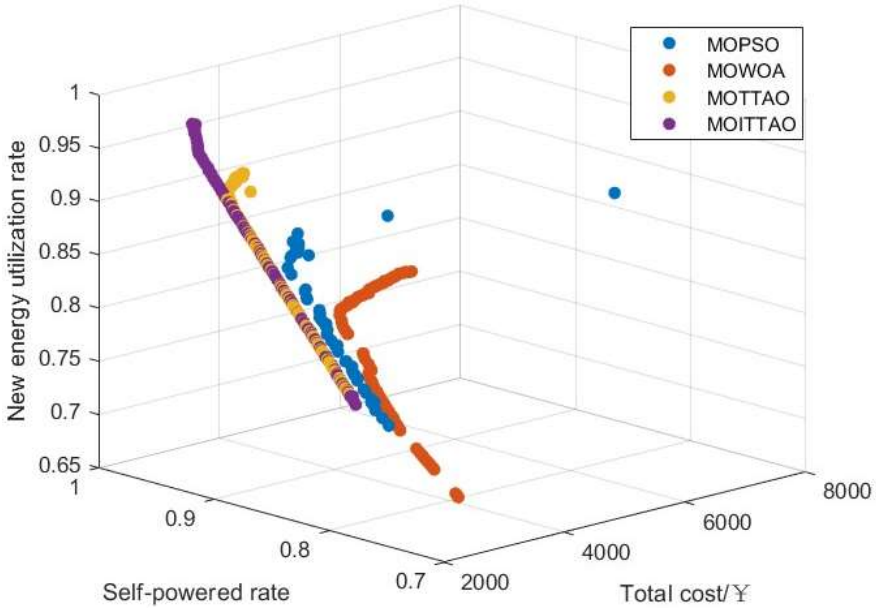

Figure 15. Pareto solution set comparison.

Combining Figures 12–15, when multi-objective ES capacity allocation is performed under the same conditions, the optimization results of the improved triangular topology optimizer are optimal for both maximization and minimization objectives, and the quality of the Pareto solution set is better than that of the other three algorithms.

The analysis of the best solutions from various algorithms for each of the three objectives is illustrated in Table 5. The table indicates that relative to MOPSO, MOWOA, and MOTTAO, the best solutions achieved by MITTAO for average daily investment are decreased by 194.62, 281.17, and 33.94, respectively. Furthermore, the solutions concerning the self-power supply rate show an enhancement of 8.99%, 9.87%, and 2.35%, respectively, while the new energy utilization rate has increased by 6.66%, 12.92%, and 4.25%. MITTAO exhibits certain advantages in addressing both maximum and minimum values.

Table 5. Comparison of different algorithms.

Algorithm	Average Daily Investment/CNY	Self-Powered Rate	New Energy Utilization Rate
MOPSO	2522.20	91.01%	88.52%
MOWOA	2608.75	90.13%	82.26%
MOTTAO	2361.52	97.65%	90.93%
MOITTAO	2327.58	100.00%	95.18%

The box plots of the optimal compromise solutions for each objective, generated by optimizing different algorithms 20 times each, are presented in Figure 16. The analysis indicates that MOITTAO demonstrates strong and consistent convergence.

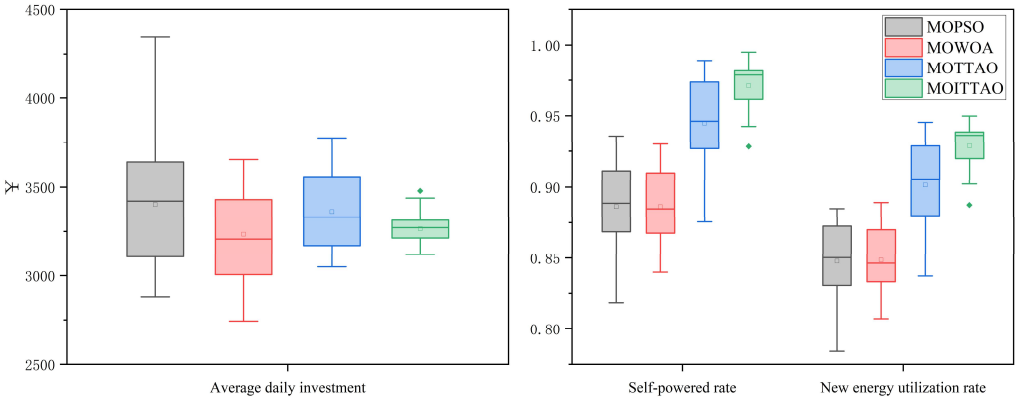

Figure 16. Box plots of the optimal compromise solutions for each objective.

Figure 17 displays the Pareto solution set derived from utilizing MOITTAO to address energy storage configuration scenarios involving both disorderly and orderly charging of EVs. The compromise optimal solution is determined using the TOPSIS method and is detailed in Table 6.

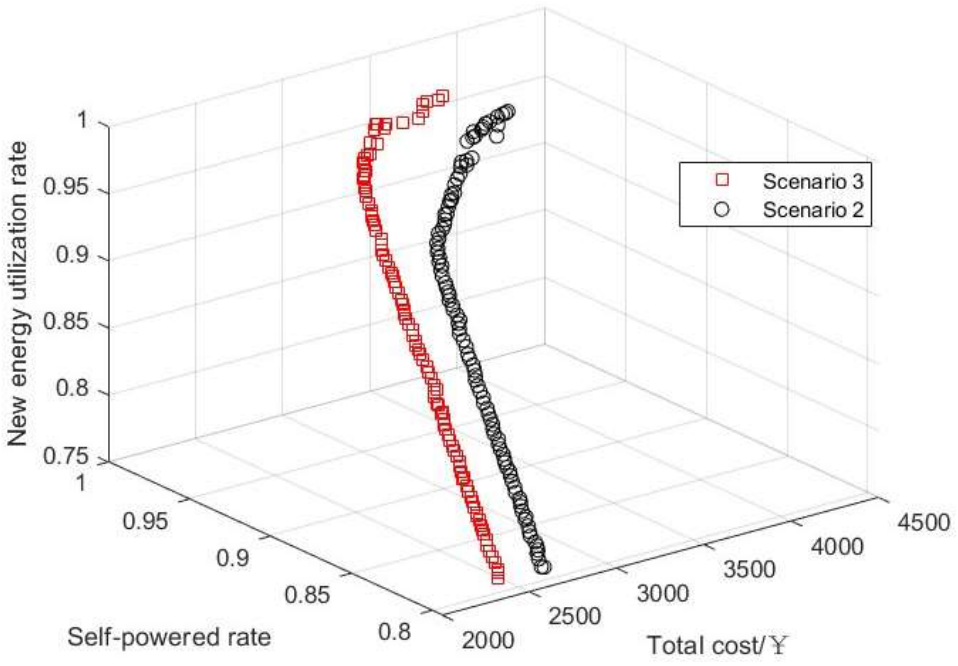

Figure 17. Pareto solution set obtained by MOITTAO.

Table 6. Comparison of energy storage capacity configurations of different scenarios.

Program	ES Capacity/kWh	Average Daily Investment/CNY	Self-Powered Rate	New Energy Utilization Rate
Scenario 1	-	-	70.38%	68.25%
Scenario 2	6701	3659.48	97.14%	92.42%
Scenario 3	6687	3454.54	99.39%	94.92%

Figure 17 and Table 6 illustrate the Pareto solution, achieved by first optimizing the charging behavior of EVs and then configuring the ES system, which surpasses that of the pre-optimization state. Following the selection of the compromise optimal solution through the TOPSIS method, Scenarios 2 and 3 are set up with approximately equivalent energy storage capacities; however, the discrepancy in average daily costs is more significant, with the self-power supply rate rising by 2.25% and the new energy utilization rate increasing by 2.50%. The optimization of EV charging behavior effectively reduces the load standard deviation in the overall system load while simultaneously enhancing the operation of the ESS. In comparison to the scenario lacking an energy storage system, both the self-powered rate and the new energy utilization rate show significant improvements following the ES system configuration. In the cases of disorderly and orderly EV charging, the self-powered rates increase by 26.76% and 29.01%, respectively; meanwhile, the new energy utilization rates rise by 24.17% and 26.67%.

Figures 18 and 19 illustrate the power balance diagrams for Scenarios 2 and 3. Figures 20 and 21 depict the SOC of the two scenarios. Analysis reveals that from 1:00 to 5:00, the combined output of Wind-PV is insufficient to meet the load power demand. During this period, the ESS is continuously discharging. Between 8:00 and 17:00, the new energy generation exceeds the system's load power, allowing the energy storage battery to charge during this time, leading to excess power generation that may be wasted. From 18:00 to 24:00, the new energy generation gradually decreases, the ESS discharges again to supply power, and when the ESS cannot fulfill the demand, power must be purchased from the grid.

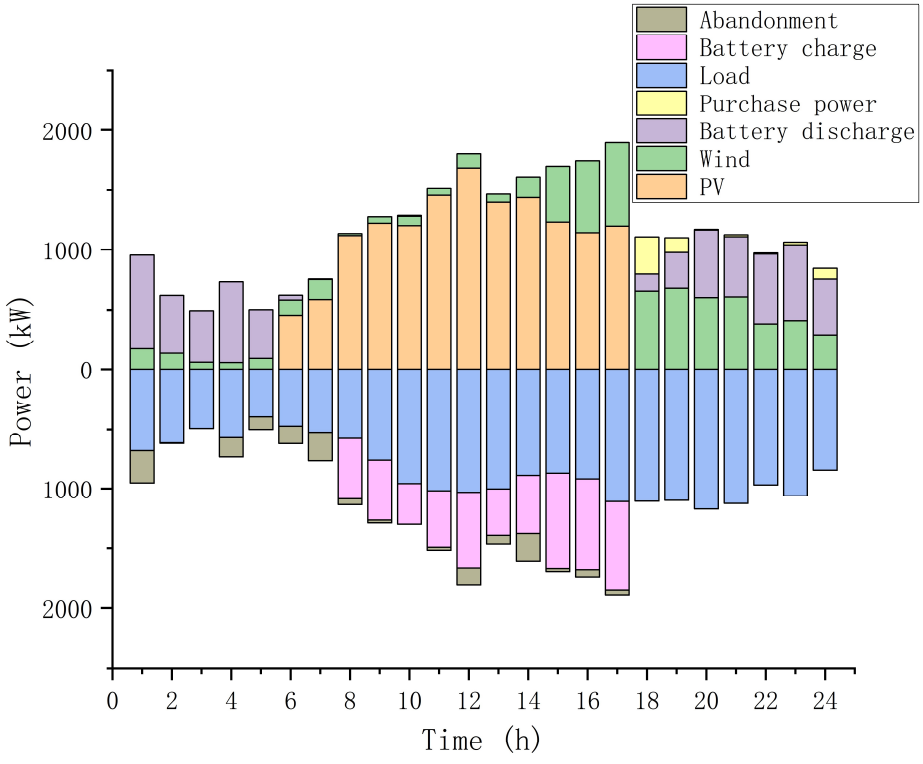

Figure 18. Power balance diagram of Scenario 2.

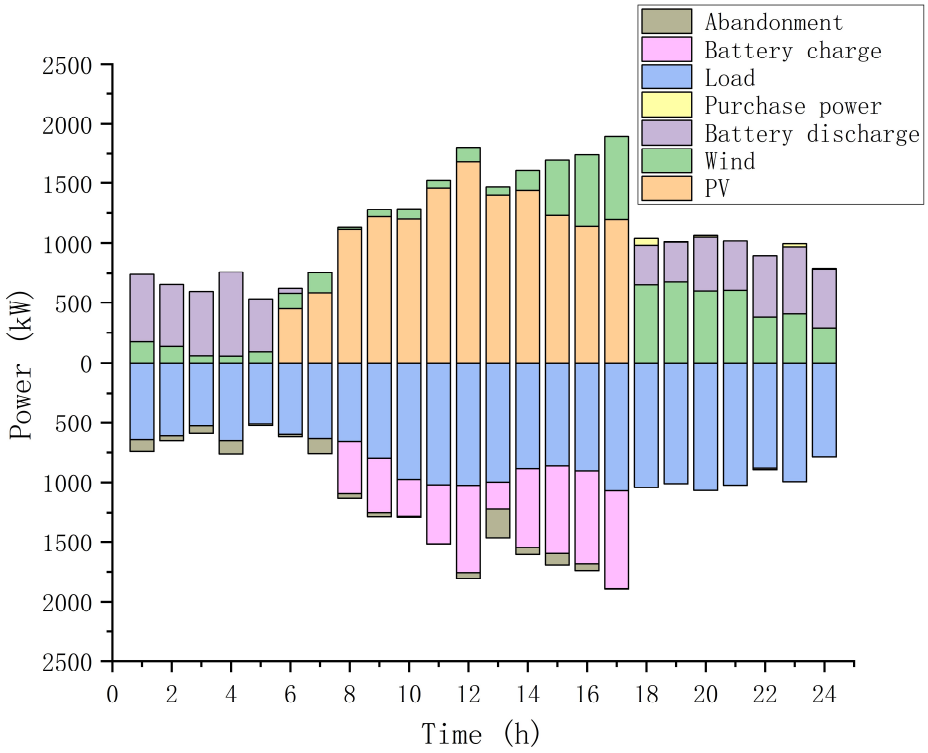

Figure 19. Power balance diagram of Scenario 3.

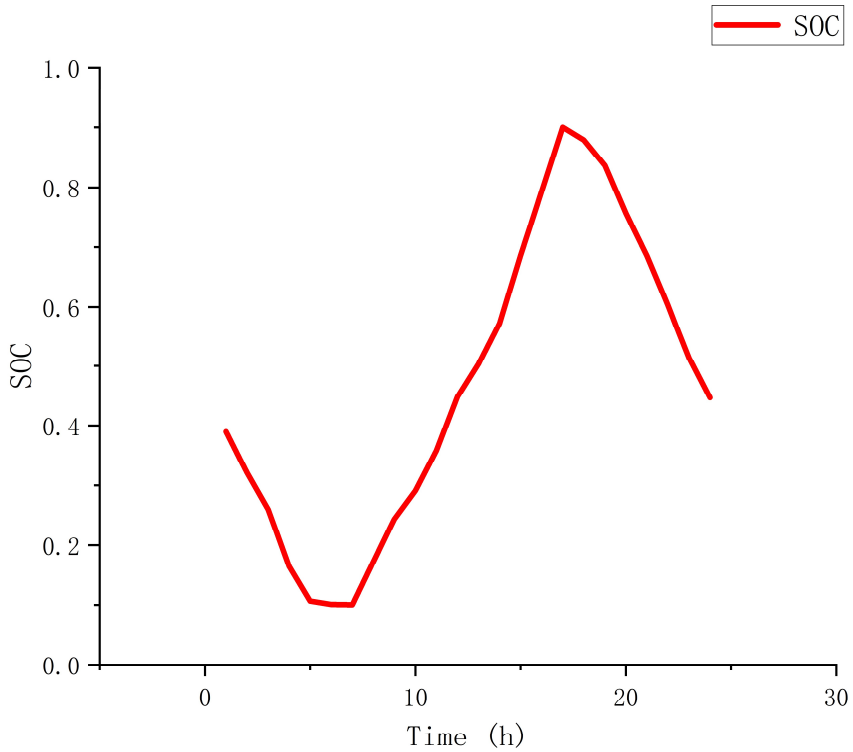

Figure 20. SOC of Scenario 2.

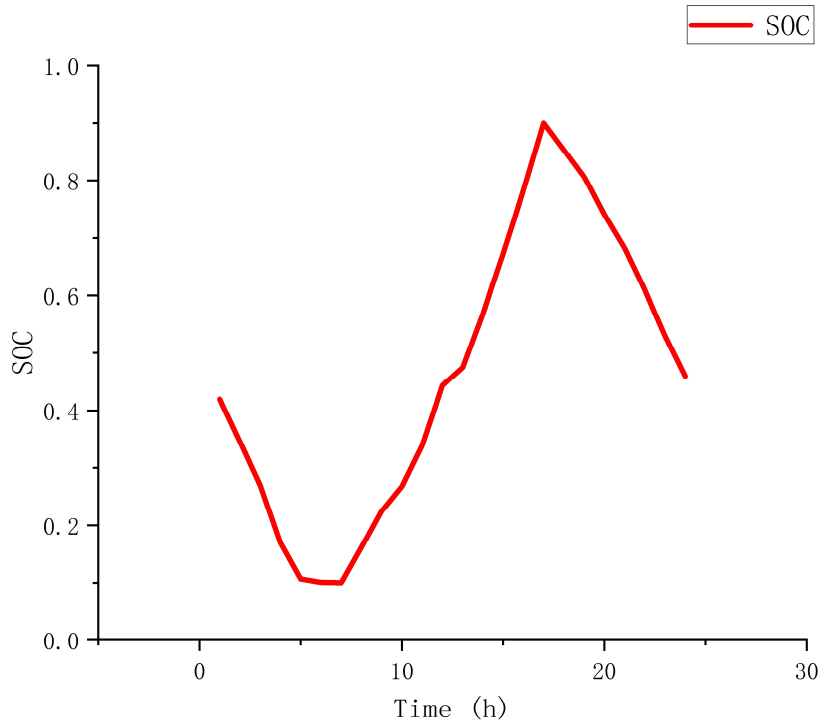

Figure 21. SOC of Scenario 3.

Analysis indicates that, in the case of EV disorderly charging, the hours from 18:00 to 24:00 represent the peak EV charging period, during which more power is purchased from the system. Electricity prices during this time are also elevated, resulting in higher purchasing costs. In contrast, electricity purchases primarily occur at 18:00 in the case of EV disorderly charging, where the purchasing cost is lower. The optimized SOC curves for both schemes are nearly identical, and their energy storage capacities are similar. However, the optimized self-power supply rate and new energy utilization rate are higher, while the average daily investment is lower.

In conclusion, employing the scenario generation and clustering method based on MCS and BR enables effective scenario analysis. By optimizing the charging behavior of EVs, the load standard deviation and user charging costs can be significantly minimized. Additionally, by combining wind power and PV supply systems that account for EV charging behavior, configuring appropriate battery storage can effectively decrease power abandonment and enhance power supply quality. However, the high cost per unit capacity of battery energy storage means that excessive energy storage can negatively impact system economics. Therefore, selecting the appropriate capacity for the ESS in the WPEES is essential.

5. Conclusions

To enhance power supply reliability and energy utilization in a new energy system that considers EV charging behavior, this paper develops a scenario analysis model utilizing MCS and BR. It investigates orderly EV charging behavior with the objectives of minimizing user charging costs and reducing the load standard deviation, proposing a multi-objective ES allocation method based on an improved TTAO. Utilizing the typical day derived from the scenario analysis, the impacts of both disorderly and orderly EV charging on the system load are examined using MCS and TTAO. The MOITTAO, enhanced by the logistic map, Gold-SA strategy, and lens imaging inverse learning strategy, is employed to solve the ES optimization configuration model. The following conclusions are derived from the analysis:

(1) Optimizing the charging behavior of electric vehicles using time-of-use tariffs can significantly lower load standard deviation and reduce user charging costs;

(2) By employing an ES allocation model that accounts for the average daily system cost, self-powered rates, and renewable energy utilization, it is possible to boost the system's self-powered rate and improve the utilization of NE while maintaining economic efficiency;
(3) The ITTAO effectively addresses sequential charging optimization and optimal ES capacity allocation for EVs. Compared to TTAO, WOA, and PSO, ITTAO enhances convergence speed while also providing a superior quality solution set.

Author Contributions: Conceptualization, H.W.; methodology, H.W. and C.F.; software, C.F.; validation, H.W. and C.F.; formal analysis, J.Z. and H.W.; investigation, C.F.; resources, H.W. and C.F.; data curation, C.F.; writing—original draft preparation, C.F.; writing—review and editing, H.W., J.Z., P.C. and Y.B.; visualization, C.F.; supervision, H.W., J.Z., P.C. and Y.B.; project administration, J.Z. and H.W.; funding acquisition, J.Z. All authors have read and agreed to the published version of the manuscript.

Funding: This work was supported in part by the National Key Research and Development Program Project (grant number: 2019YFE0104800), the Scientific and Technological Innovation Team of Colleges and Universities in Henan Province (grant number: 22IRTSTHN011), and the Scientific and Technological Research Project of Henan Provincial Department of Education (grant number: 20A210027).

Data Availability Statement: Data are contained within the article.

Conflicts of Interest: The authors declare no conflicts of interest.

Abbreviations

BR	Backward Reduction
CDF	Cumulative distribution function
cGAN	Cross-modal generative adversarial network
COS	Cost of system
ES	Energy storage
ESS	Energy storage system
EV	Electric vehicle
Gold-SA	Golden Sine Algorithm
LSD	Load standard deviation
MCS	Monte Carlo sampling
MOITTAO	Multi-objective improved TTAO
MOPSO	Multi-objective particle swarm optimization
MOTTAO	Multi-objective triangulation topology aggregation optimizer
MOWOA	Multi-objective whale optimization algorithm
NE	New energy
O&M	Operation and maintenance
PV	Photovoltaic
SOC	State of charge
TOPSIS	Technique for Order Preference by Similarity to Ideal Solution
TTAO	Triangulation topology aggregation optimizer
WPESS	Wind-PV-Energy storage system
WPEES	Wind-PV-EV-ES system

References

1. Du, X. Thoughts on strategies and paths to achieve carbon peaking and carbon neutrality in China. *Front. Energy* **2023**, *17*, 324–331. [CrossRef]
2. Winskel, M.; Kattirtzi, M. Transitions, disruptions and revolutions: Expert views on prospects for a smart and local energy revolution in the UK. *Energy Policy* **2020**, *147*, 111815. [CrossRef]
3. Luo, X.; He, Y.; Zhang, J.; Li, J. Optimal Allocation of Hybrid Energy Storage Capacity Based on ISSA-Optimized VMD Parameters. *Electronics* **2024**, *13*, 2597. [CrossRef]
4. Zhang, J.; Zhu, Y.; Zhao, Z. Optimal Scheduling Strategy for Power Systems Containing Offshore Wind Farms Considering Wind Power Uncertainty. *J. Circuits Syst. Comput.* **2022**, *32*, 2350090. [CrossRef]

5. Zhang, K.; Feng, P.; Zhang, G. Bi-level Optimization Configuration Method for Multi-Energy Microgrid Considering Chance Constraint. *Acta Energiae Solaris Sin.* **2021**, *8*, 41–48.
6. Zhang, W.; Maleki, A.; Rosen, M.A.; Liu, J. Optimization with a simulated annealing algorithm of a hybrid system for renewable energy including battery and hydrogen storage. *Energy* **2018**, *163*, 191–207. [CrossRef]
7. Nimma, K.S.; Al-Falahi, M.D.A.; Nguyen, H.D.; Jayasinghe, S.D.G.; Mahmoud, T.S.; Negnevitsky, M. Grey Wolf Optimization-Based Optimum Energy-Management and Battery-Sizing Method for Grid-Connected Microgrids. *Energies* **2018**, *11*, 847. [CrossRef]
8. Xue, Y. Energy internet or comprehensive energy network? *J. Mod. Power Syst. Clean Energy* **2015**, *3*, 297–301. [CrossRef]
9. Lv, S.; Li, J.; Guo, Y.; Shi, Z. A Typical Distributed Generation Scenario Reduction Method Based on an Improved Clustering Algorithm. *Appl. Sci.* **2019**, *9*, 4262. [CrossRef]
10. Yin, Y.; Liu, T.; He, C. Day-ahead stochastic coordinated scheduling for thermal-hydro-wind-photovoltaic systems. *Energy* **2019**, *187*, 115944. [CrossRef]
11. Zhang, J.; Meng, H.; Gu, B.; Li, P. Research on short-term wind power combined forecasting and its Gaussian cloud uncertainty to support the integration of renewables and EVs. *Renew. Energy* **2020**, *153*, 884–899. [CrossRef]
12. Meng, Q.; Tong, X.; Hussain, S.; Luo, F.; Zhou, F.; Liu, L.; He, Y.; Jin, X.; Li, B. Revolutionizing photovoltaic consumption and electric vehicle charging: A novel approach for residential distribution systems. *IET Gener. Transm. Distrib.* **2024**, *18*, 2822–2833. [CrossRef]
13. Yin, W.; Ming, Z.; Wen, T. Scheduling strategy of electric vehicle charging considering different requirements of grid and users. *Energy* **2021**, *232*, 121118. [CrossRef]
14. Meng, Q.; Hussain, S.; Luo, F.; Wang, Z.; Jin, X. An Online Reinforcement Learning-based Energy Management Strategy for Microgrids with Centralized Control. *IEEE Trans. Ind. Appl.* **2024**, 1–10. [CrossRef]
15. Rekioua, D. Energy Storage Systems for Photovoltaic and Wind Systems: A Review. *Energies* **2023**, *16*, 3893. [CrossRef]
16. Fu, H.; Shi, M.; Feng, M. Capacity optimization strategy for energy storage system to ensure power supply. *Int. J. Low-Carbon Technol.* **2023**, *18*, 622–627. [CrossRef]
17. Fakih, S.; Mabrouk, M.T.; Batton-Hubert, M.; Lacarriere, B. Bi-level and multi-objective optimization of renewable energy sources and storage planning to support existing overloaded electricity grids. *Energy Rep.* **2023**, *10*, 1450–1466. [CrossRef]
18. Fan, W.; Tan, Q.; Zhang, A.; Ju, L.; Wang, Y.; Yin, Z.; Li, X. A Bi-level optimization model of integrated energy system considering wind power uncertainty. *Renew. Energy* **2023**, *202*, 973–991. [CrossRef]
19. Ramli, M.a.M.; Bouchekara, H.R.E.H.; Alghamdi, A.S. Optimal sizing of PV/wind/diesel hybrid microgrid system using multi-objective self-adaptive differential evolution algorithm. *Renew. Energy* **2018**, *121*, 400–411. [CrossRef]
20. Zhao, S.; Zhang, T.; Cai, L.; Yang, R. Triangulation topology aggregation optimizer: A novel mathematics-based meta-heuristic algorithm for continuous optimization and engineering applications. *Expert Syst. Appl.* **2024**, *238*, 121744. [CrossRef]
21. Dong, G.; Chen, Z.; Wei, J. Sequential Monte Carlo Filter for State-of-Charge Estimation of Lithium-Ion Batteries Based on Auto Regressive Exogenous Model. *IEEE Trans. Ind. Electron.* **2019**, *66*, 8533–8544. [CrossRef]
22. Li, J.; Zhou, J.; Chen, B. Review of wind power scenario generation methods for optimal operation of renewable energy systems. *Appl. Energy* **2020**, *280*, 115992. [CrossRef]
23. Razali, N.M.M.; Hashim, A.H. Backward reduction application for minimizing wind power scenarios in stochastic programming. In Proceedings of the 2010 4th International Power Engineering and Optimization Conference (PEOCO), Selangor, Malaysia, 23–24 June 2010; pp. 430–434.
24. Henrion, R.; Küchler, C.; Roemisch, W. Discrepancy distances and scenario reduction in two-stage stochastic mixed-integer programming. *J. Ind. Manag. Optim.* **2008**, *4*, 363–384. [CrossRef]
25. Usta, I.; Arik, I.; Yenilmez, I.; Kantar, Y.M. A new estimation approach based on moments for estimating Weibull parameters in wind power applications. *Energy Convers. Manag.* **2018**, *164*, 570–578. [CrossRef]
26. Sumair, M.; Aized, T.; Bhutta, M.M.A.; Siddiqui, F.A.; Tehreem, L.; Chaudhry, A. Method of Four Moments Mixture-A new approach for parametric estimation of Weibull Probability Distribution for wind potential estimation applications. *Renew. Energy* **2022**, *191*, 291–304. [CrossRef]
27. Wais, P. A review of Weibull functions in wind sector. *Renew. Sustain. Energy Rev.* **2017**, *70*, 1099–1107. [CrossRef]
28. Tiam Kapen, P.; Jeutho Gouajio, M.; Yemélé, D. Analysis and efficient comparison of ten numerical methods in estimating Weibull parameters for wind energy potential: Application to the city of Bafoussam, Cameroon. *Renew. Energy* **2020**, *159*, 1188–1198. [CrossRef]
29. Zhang, J.; Yan, J.; Infield, D.; Liu, Y.; Lien, F.-S. Short-term forecasting and uncertainty analysis of wind turbine power based on long short-term memory network and Gaussian mixture model. *Appl. Energy* **2019**, *241*, 229–244. [CrossRef]
30. Luo, Y.; Nie, Q.; Yang, D.; Zhou, B. Robust Optimal Operation of Active Distribution Network Based on Minimum Confidence Interval of Distributed Energy Beta Distribution. *J. Mod. Power Syst. Clean Energy* **2021**, *9*, 423–430. [CrossRef]
31. Fernandez-Jimenez, L.A.; Monteiro, C.; Ramirez-Rosado, I.J. Short-term probabilistic forecasting models using Beta distributions for photovoltaic plants. *Energy Rep.* **2023**, *9*, 495–502. [CrossRef]
32. Mcguckin, N.; Fucci, A. Summary of Travel Trends: 2017 National Household Travel Survey. 2018. Available online: https://rosap.ntl.bts.gov/view/dot/68751 (accessed on 31 August 2024).

33. Du, W.; Ma, J.; Yin, W. Orderly charging strategy of electric vehicle based on improved PSO algorithm. *Energy* **2023**, *271*, 127088. [CrossRef]
34. Zhao, D.; Wang, H.; Huang, J.; Lin, X. Time-of-Use Pricing for Energy Storage Investment. *IEEE Trans. Smart Grid* **2022**, *13*, 1165–1177. [CrossRef]
35. Guo, J.; Zhang, P.; Wu, D.; Liu, Z.; Ge, H.; Zhang, S.; Yang, X. A new collaborative optimization method for a distributed energy system combining hybrid energy storage. *Sustain. Cities Soc.* **2021**, *75*, 103330. [CrossRef]
36. Yi, T.; Ye, H.; Li, Q.; Zhang, C.; Ren, W.; Tao, Z. Energy storage capacity optimization of wind-energy storage hybrid power plant based on dynamic control strategy. *J. Energy Storage* **2022**, *55*, 105372. [CrossRef]
37. Li, D.; Cai, W. Optimal configuration of photovoltaic energy storage capacity for large power users. *Energy Rep.* **2021**, *7*, 468–478. [CrossRef]
38. Mah, A.X.Y.; Ho, W.S.; Hassim, M.H.; Hashim, H.; Ling, G.H.T.; Ho, C.S.; Ab Muis, Z. Optimization of photovoltaic-based microgrid with hybrid energy storage: A P-graph approach. *Energy* **2021**, *233*, 121088. [CrossRef]
39. Yang, B.; Liao, X. Some properties of the Logistic map over the finite field and its application. *Signal Process.* **2018**, *153*, 231–242. [CrossRef]
40. Tanyildizi, E.; Demir, G. Golden Sine Algorithm: A Novel Math-Inspired Algorithm. *Adv. Electr. Comput. Eng.* **2017**, *17*, 71–78. [CrossRef]
41. Tizhoosh, H.R. Opposition-Based Reinforcement Learning. *J. Adv. Comput. Intell. Intell. Inform.* **2006**, *10*, 578–585. [CrossRef]
42. Zhang, J.; Xue, X.; Li, D.; Yan, J.; Cheng, P. Optimization of Energy Storage Allocation in Wind Energy Storage Combined System Based on Improved Sand Cat Swarm Optimization Algorithm. *Processes* **2023**, *11*, 3274. [CrossRef]
43. Wang, J.-J.; Jing, Y.-Y.; Zhang, C.-F.; Zhao, J.-H. Review on multi-criteria decision analysis aid in sustainable energy decision-making. *Renew. Sustain. Energy Rev.* **2009**, *13*, 2263–2278. [CrossRef]